nature communications

Article

https://doi.org/10.1038/s41467-024-53960-5

Oriented triplex DNA as a synthetic receptor for transmembrane signal transduction

Received: 19 June 2024

Accepted: 29 October 2024

Published online: 12 November 2024

Check for updates

Hui Chen, Shaohong Zhou, Kleins Ngocho, Jing Zheng, Xiaoxiao He, Jin Huang, Kemin Wang, Hui Shi & Jianbo Liu

Signal transduction across biological membranes enables cells to detect and respond to diverse chemical or physical signals, and replicating these complex biological processes through synthetic methods is of significant interest in synthetic biology. Here we present an artificial signal transduction system using oriented cholesterol-tagged triplex DNA (TD) as synthetic receptors to transmit and amplify signals across lipid bilayer membranes through H^+-mediated TD conformational transitions from duplex to triplex. An auxiliary sequence, complementary to the third strand of the TD, ensures a controlled and preferred outward orientation of cholesterol-tagged TD on membranes. Upon external H^+ stimuli, the conformational change triggers the translocation of the third strand from the outer to the inner membrane leaflet, resulting in effective transmembrane signal transduction. This mechanism enables fluorescence resonance energy transfer (FRET), selective photocleavage, catalytic signal amplification, and logic gate modulation within vesicles. Our findings demonstrate that these TD-based receptors mimic the functional dynamics of natural G protein-coupled receptors (GPCRs), providing a foundation for advanced applications in biosensing, cell signaling modulation, and targeted drug delivery systems.

Transmembrane signal transduction is a fundamental biological process involving the transmission of signals across cell membranes through membrane-spanning protein receptors, which subsequently initiate a series of biochemical reaction cascades within cells[1,2]. Studying chemical systems that replicate signal transduction in synthetic cells is crucial not only for understanding life processes but also holds significant promise in synthetic biology, bioengineering, materials science, and origin of life research[3–5]. Natural cells decode external signals using surface membrane receptors like receptor tyrosine kinases (RTKs) and G protein-coupled receptors (GPCRs). RTKs operate through ligand-induced dimerization of transmembrane units[6], while GPCRs involve global conformational changes that activate intracellular signaling cascades[7]. Both pathways effectively transduce signals without mass exchange across lipid bilayers, thus maintaining cellular integrity and preventing the entry of harmful substances[8]. While synthetic systems that mimic RTK signaling via organic molecule dimers[9–11] or DNA nanostructures[12,13] have been developed, emulating GPCR-like global conformational transitions for signal transduction remains more challenging. In a pioneering study, Clayden et al. developed helical peptide foldamers that mimic GPCRs, where chirality changes were induced by the recognition of chiral ligands[14,15]. These peptide foldamers displayed light-mediated global conformational changes on membranes, facilitating transmembrane signaling[16,17]. Additionally, Hunter et al. reported an abiotic transmembrane signal transduction mechanism in which receptor activation by organic molecules prompted the cross-membrane movement of the receptor, thereby exposing metalloenzymes for signal amplification[18–21]. However, organic molecules and short peptide-based mimics of membrane receptors often face limitations in achieving controlled membrane orientation and design flexibility.

DNA nanostructures have emerged as powerful tools in the design of artificial systems due to their programmability, controllability, and structural specificity[22–25]. Membrane-spanning synthetic receptors

State Key Laboratory of Chemo/Biosensing and Chemometrics, College of Chemistry and Chemical Engineering, Key Laboratory for Bio-Nanotechnology and Molecular Engineering of Hunan Province, Hunan University, Changsha, People's Republic of China. e-mail: liujianbo@hnu.edu.cn

https://doi.org/10.1038/s41467-024-53960-5

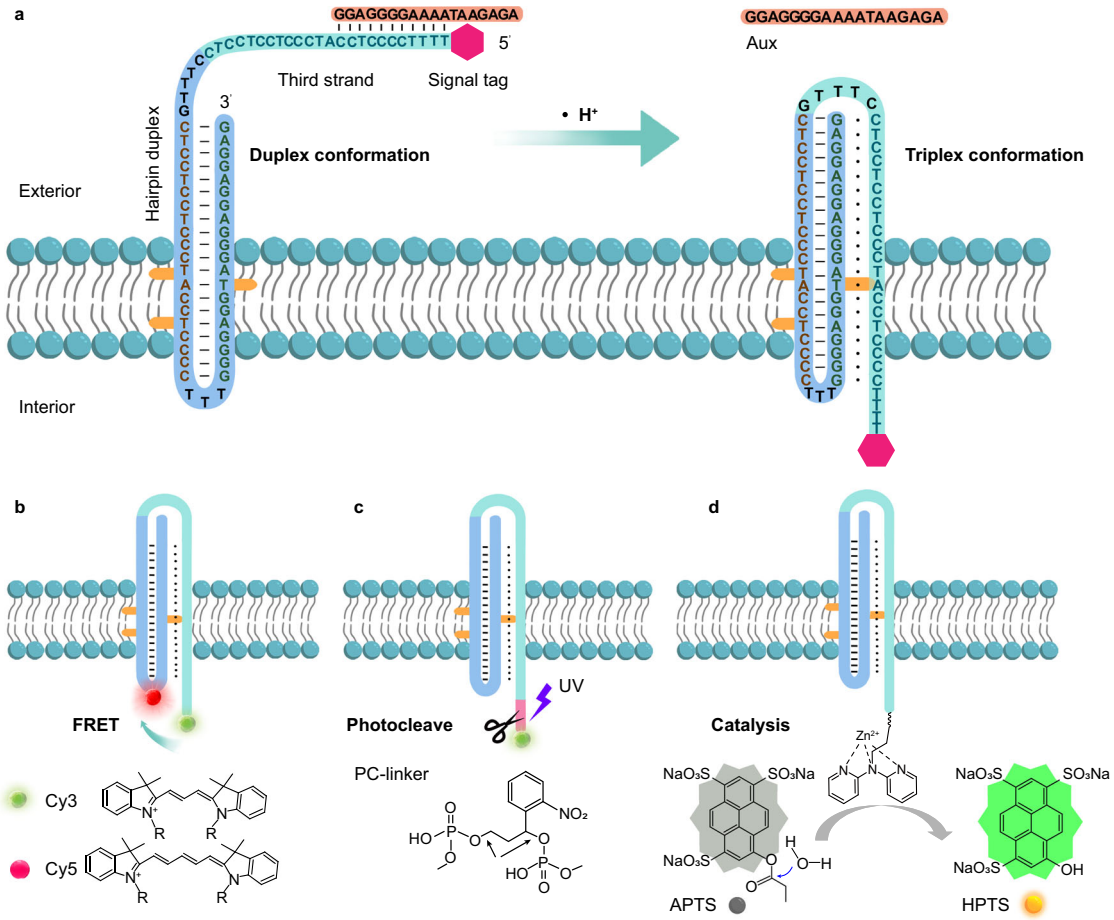

Fig. 1 | Oriented triplex DNA (TD) as a synthetic receptor for transmembrane signal transduction. a Schematic illustration of TD assembly on a lipid bilayer membrane, showing the H^+-induced conformational transition from duplex to triplex. Three cholesterols (khaki) conjugated to the stem of the TD hairpin anchor the TD across the bilayer membrane. An auxiliary sequence (Aux_n, $n = 11$), complementary to the third strand, acts as a steric hindrance module to ensure the outward orientation of the TD on the membrane. Upon lowering the pH, the conformational change from duplex to triplex is coupled with the translocation of the signal tags from the exterior to the interior of the membrane, facilitating signal transduction and amplification across the membrane. Low pH triggers triplex formation and subsequent transmembrane signal transduction, observed as: (**b**) Fluorescence resonance energy transfer (FRET) occurrence, bringing Cy3 and Cy5 into proximity. **c** Photocleavage reactions accompanying signal module translocation into the membrane interior, leading to fluorescence emission within vesicles. **d** Catalytic conversion of the non-fluorescent ester substrate 8-acetoxypyrene-1,3,6-trisulfonatetrisodium salt (APTS) into the fluorescent product 8-hydroxypyrene-1,3,6-trisulfonatetrisodium salt (HPTS) upon internalization of the procatalyst dipyridylamine tagged to the 5′-terminus of TD.

have been constructed from various DNA configurations, including multiple duplex sequences and noncanonical nucleic acids like i-motifs and G-quadruplexes[26,27]. These DNA-based receptors can transduce and amplify chemical signals across bilayer membranes. Triplex DNA (TD), composed of purine-rich or pyrimidine-rich oligonucleotides, undergoes pH-dependent conformational changes from duplex to triplex[28–30], very mimicking the dynamic response seen in GPCRs. Given their ability to undergo significant conformational transitions, TD structures are promising candidates for designing synthetic receptors that can emulate GPCR-like signal transduction. The development of active artificial receptors would promote signal communication within model cells and reinforce their reception, transduction, and response to environmental stimuli.

In this study, we introduce a TD-based synthetic transmembrane signal receptor system that leverages H^+-induced conformational changes to achieve effective signal transduction and catalytic amplification within vesicles (Fig. 1a). The synthetic receptor, designed to transition from a duplex to a triplex conformation in response to external H^+ ions, is anchored across lipid bilayer membranes using hydrophobic cholesterols. An auxiliary sequence complementary to the third strand of the TD facilitates a preferred outward orientation, ensuring efficient membrane integration and functionality. Upon H^+ stimulation, the conformational change from duplex to triplex triggers the translocation of the third strand from the outer to the inner leaflet of the membrane. This translocation leads to transmembrane fluorescence resonance energy transfer (FRET), selective photocleavage, and catalytic signal amplification (Fig. 1b–d), mimicking the intricate signaling mechanisms of natural GPCRs. Finally, AND Boolean logic gates for transmembrane signal transduction were established by increasing the number of nucleotides in the auxiliary sequences. Our findings highlight the potential of TD-based synthetic receptors to function as versatile tools for biosensing, cell signaling modulation, and targeted drug delivery. By integrating modular design principles and controllable conformational dynamics, this approach represents a significant step toward creating sophisticated synthetic signaling networks that can respond to environmental stimuli and facilitate complex intracellular communication.

Results

Membrane insertion and auxiliary sequence-mediated outward orientation of synthetic receptors

The design of triplex DNA (TD)-based synthetic transmembrane receptors involves three key functional modules: a stimulus-responsive TD structure capable of pH-dependent conformational

https://doi.org/10.1038/s41467-024-53960-5

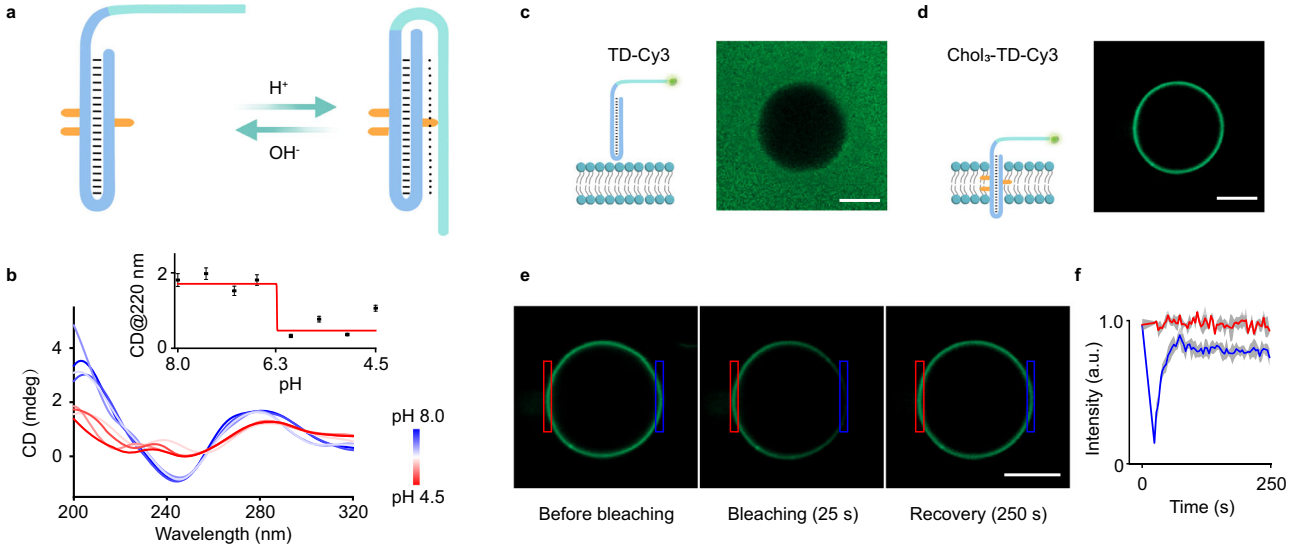

Fig. 2 | pH-activable conformational change and membrane insertion of cholesterol-tagged TD. a Schematic diagram showing the pH-dependent conformational transition of cholesterol-tagged TD. **b** CD spectra depicting the duplex to triplex transition of cholesterol-tagged TD as the pH is lowered from 8.0 to 4.5. Inset: Quantitative analysis of the CD intensity at 220 nm. Data are presented as mean ± s.d. ($n = 3$ independent experiments). Confocal fluorescence images of a single GUV incubated with (**c**) cholesterol-tagged $Chol_3$-TD-Cy3 and (**d**) cholesterol-free TD-Cy3. Each experiment was independently repeated three times, with consistent results (**c**, **d**). Scale bar, 5 μm. **e**, **f** FRAP measurements of membrane fluidity. Confocal fluorescence images of a single vesicle membrane doped with $Chol_3$-TD-Cy3 at different time intervals (**e**) and corresponding fluorescence intensity changes (**f**) recorded before and after photobleaching. The photobleached area is delineated by the blue box in (**e**) and corresponds to the blue plot in (**f**). Data in (**f**) are presented as mean ± s.d. ($n = 3$ independent GUVs). TD, $Chol_3$-TD: 1 μM; vesicle: 1 mM lipid. Scale bar, 5 μm. a.u. arbitrary units.

changes, a hydrophobic segment that anchors the receptor across the membrane, and a signal output module for fluorescence production or activation of cascade reactions within vesicles. We employed a C-base-rich TD sequence as the scaffold for our synthetic receptors, demonstrating a reversible conformational change between duplex and triplex states within a pH range of 5.5–7.5 (Fig. 2a). To characterize the conformational transformation of cholesterol-tagged TD in a homogeneous buffer, we performed pH-dependent circular dichroism (CD) spectroscopy (Fig. 2b and Supplementary Fig. 2). As the ambient pH was lowered from 8.0 to 4.5, we observed a significant shift in the CD spectrum below pH 6.2, indicating the transition from a hairpin duplex to a triplex conformation. This was evidenced by a redshift in the characteristic CD peak from 245 nm to 252 nm, while the positive peak at 280 nm remained unchanged. Additionally, a new negative shoulder peak emerged at 220 nm, characteristic of triplex DNA[31] (Fig. 2b).

Effective insertion and orientation of TD on lipid bilayers are crucial for designing synthetic membrane receptors. To facilitate membrane anchoring, we tagged cholesterols to the middle of the TD, resulting in bright fluorescent rings at the periphery of giant unilamellar vesicles (GUVs) observed under confocal fluorescent imaging (Fig. 2d and Supplementary Fig. 3). As a control, GUVs with cholesterol-free TD remained dark (Fig. 2c). Fluorescence recovery after photobleaching (FRAP) experiments showed 92% fluorescence recovery in the bleached region within 250 s, confirming the membrane fluidity, that is crucial for translocation of cholesterol-tagged TD across bilayer membranes (Fig. 2e, f). The number of cholesterols tagged on the TD significantly impacted their orientation on the membrane. Linear dichroism (LD) spectra were used to assess the orientation of TDs ($Chol_n$-TD, $n = 0–3$) relative to the lipid membrane. $Chol_2$-TD and $Chol_3$-TD exhibited positive peaks at 260 nm, indicating a perpendicular orientation on the membrane, whereas $Chol_0$-TD and $Chol_1$-TD showed no obvious LD peak, suggesting no adhesion or a flat orientation on the lipid membranes[32,33] (Supplementary Fig. 4). Among these, $Chol_3$-TD displayed the highest linear dichroism intensity and was used for further studies.

Upon immobilization on the lipid bilayer membrane, the inherent fluidity of the bilayer could cause the translocation of the cholesterol-tagged TD, resulting in random orientations, including both outward and inward directions (Fig. 3a). Previous studies have demonstrated that asymmetric DNA nanostructures with significant steric hindrance can be directionally assembled on membranes in a preferred orientation[34]. To enhance the outward orientation of TD on the membrane, we incorporated an auxiliary sequence that is partly complementary to the third strand, positioned on the exterior of the membrane. This auxiliary sequence acts as a steric hindrance or hydrophilic domain, preventing random translocation of the synthetic receptors and promoting a controlled, outward orientation.

The oriented outward assembly of cholesterol-tagged TD on membranes was evaluated using a nuclease digestion fluorescence assay[35,36]. In this assay, cholesterol-tagged TD inserted into the bilayer membrane are partially shielded from nuclease digestion, whereas those in solution are fully accessible (Supplementary Fig. 5–7). As shown in Fig. 3b, after immobilization of Cy3-labeled $Chol_3$-TD on membranes, the addition of DNase I resulted in a gradual decrease in fluorescence on the GUVs. The fluorescence intensity decayed to 35% within 600 s (Fig. 3c and Supplementary Fig. 8a), attributed to the digestion of outward-oriented TD exposed on the membrane exterior, while inward-oriented TD remained protected from digestion. In contrast, in the presence of the auxiliary sequence (Aux_{11}) (Fig. 3d), the fluorescence intensity decayed rapidly, decreasing by nearly 99% within 600 s (Fig. 3e–f and Supplementary Fig. 8b). This increased rate of fluorescence attenuation indicates that the auxiliary sequence significantly improved the outward orientation of $Chol_3$-TD. Combined with fluorescence recovery experiments (Supplementary Fig. 9), the proportion of outward-oriented $Chol_3$-TD was determined to increase up to 99.0% in the presence of the auxiliary sequence (Fig. 3g–j), suggesting nearly complete outward orientation for the synthetic receptors.

H^+-mediated conformational change of TD receptors for transmembrane FRET and photocleavage

We examined the H^+-mediated transition from duplex to triplex in TD at the membrane interface using a FRET assay (Fig. 4a). Cy3 and Cy5, serving as the FRET donor and acceptor, were labeled at the

https://doi.org/10.1038/s41467-024-53960-5

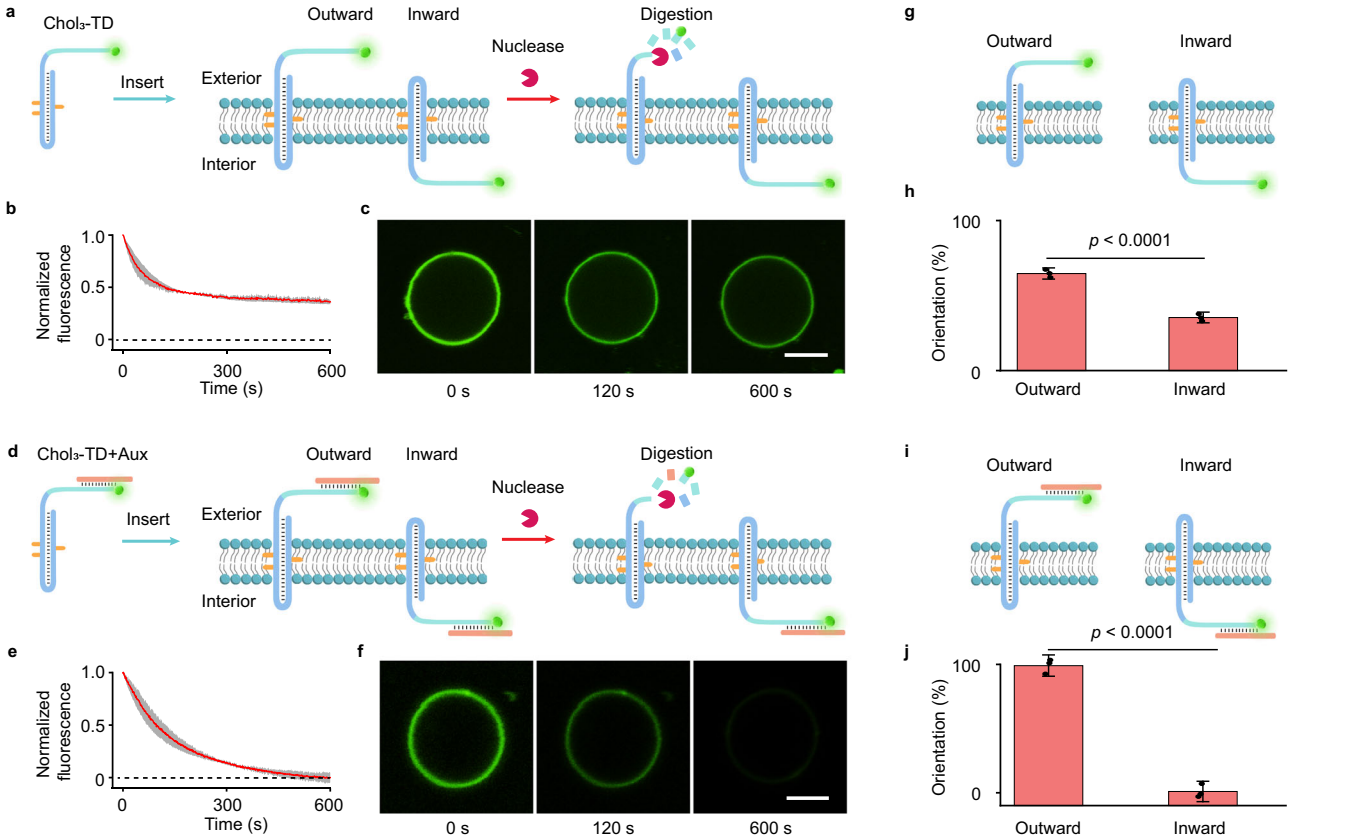

Fig. 3 | Auxiliary sequence-mediated outward orientation of cholesterol-tagged TD on membrane. Schematic diagrams of the nuclease degradation experiment for $Chol_3$-TD in vesicle suspensions without (**a**) and with (**d**) the auxiliary sequence (Aux_{11}). **b**, **e** Fluorescence kinetic curves and (**c**, **f**) confocal images of $Chol_3$-TD immobilized on vesicles subjected to DNase I digestion in the absence (**b**, **c**) and presence (**e**, **f**) of the auxiliary sequence (Aux_{11}). Cy3 was tagged at the 5′-terminus of $Chol_3$-TD. The dotted line in (**b**, **e**) represents the baseline for complete nuclease degradation of the cholesterol-tagged TD. The fluorescence kinetic experiments were conducted in 200 nm LUVs, and the confocal imaging experiments were conducted in GUVs. Data in (**b**, **e**) are presented as mean ± s.d. ($n = 3$ independent LUV samples). Each experiment was independently repeated three times, with consistent results (**c**, **f**). Scale bar (**c**, **f**), 5.0 μm. **g**–**j** Quantification of $Chol_3$-TD orientation on membranes without (**g**, **h**) and with (**i**, **j**) the auxiliary sequence. Data in (**h**, **j**) are presented as mean ± s.d., two-sided Student's t-test ($n = 3$ independent experiments). TD concentration: 1 μM; vesicle lipid concentration: 1 mM; DNase I: 5.0 U; Aux_{11}: 5 μM.

5′-terminus and the loop of the hairpin duplex, respectively. These TD constructs were incubated with GUVs to achieve oriented membrane immobilization, facilitated by the auxiliary sequence. The normalized fluorescence spectra (Fig. 4b) demonstrated an increase in fluorescence at 675 nm as the pH decreased from 8.0 to 5.0, reflecting a 14.7-fold rise in FRET efficiency (Fa/Fd ratio). This increase in FRET indicates the conformational shift and triplex formation. Confocal fluorescence imaging of individual GUVs also confirmed that low-pH conditions induce conformational changes and FRET across the membrane, with a pronounced FRET signal from Cy5 fluorescence observed at pH 5.5 (Fig. 4c and Supplementary Fig. 10). The FRET results at the membrane interface were consistent with those in a homogeneous solution, with an inflection point for conformational transformation at pH 6.0 (Supplementary Fig. 11). As a control, no FRET signal was detected when the third strand was replaced with a random sequence (Supplementary Fig. 12). The conformational transformation involves the detachment of the auxiliary strand followed by subsequent transmembrane translocation. Confocal imaging revealed that upon the addition of H^+ ions, the auxiliary strand (Aux_{11}) detached from the TD receptors, leading to a rapid decrease in fluorescence intensity on the membrane (Supplementary Fig. 13). This transmembrane translocation is a rapid dynamic process, occurring within approximately 120 s following the addition of H^+ (Supplementary Fig. 14). Moreover, our findings indicate that the toehold sequence on the TD receptor, which is exposed to the duplex backbone of the outer membrane leaflet, plays a crucial role in the transmembrane translocation. No significant FRET signal or transmembrane translocation was observed when the toehold sequence was replaced with a non-binding sequence (Supplementary Fig. 15). At least 8 nt toehold sequence in the third strand was required for the effective transmembrane translocation (Supplementary Fig. 16). We hypothesize that the third strand binds with the toehold sequence through hoogsteen base pairing on the duplex, and this toehold-mediated binding facilitates the complete translocation of the signal module on the third strand from the outer to the inner leaflet of the membrane.

To verify that triplex formation mediates the transmembrane translocation of the signal module, we utilized a photocleavable linker (PC-linker) attached to the third strand as a photoresponsive fluorescence signal output module (Fig. 4d). At high pH (7.5), UV irradiation for 20 min led to a gradual increase in exterior fluorescence of the vesicles, with no significant change in interior fluorescence (Fig. 4e, f and Supplementary Fig. 17a–c). Conversely, at low-pH (5.5), UV irradiation resulted in a gradual increase in interior fluorescence, with no noticeable change in exterior fluorescence (Fig. 4g, h and Supplementary Fig. 17d–f). These observations indicate that the low-pH-induced conformational change and triplex formation are associated with the translocation of the signal module from the exterior to the interior of the membrane, resulting in photocleavage at different membrane leaflets. Control experiments showed no significant fluorescence changes when the PC-linker motif was not attached to the

https://doi.org/10.1038/s41467-024-53960-5

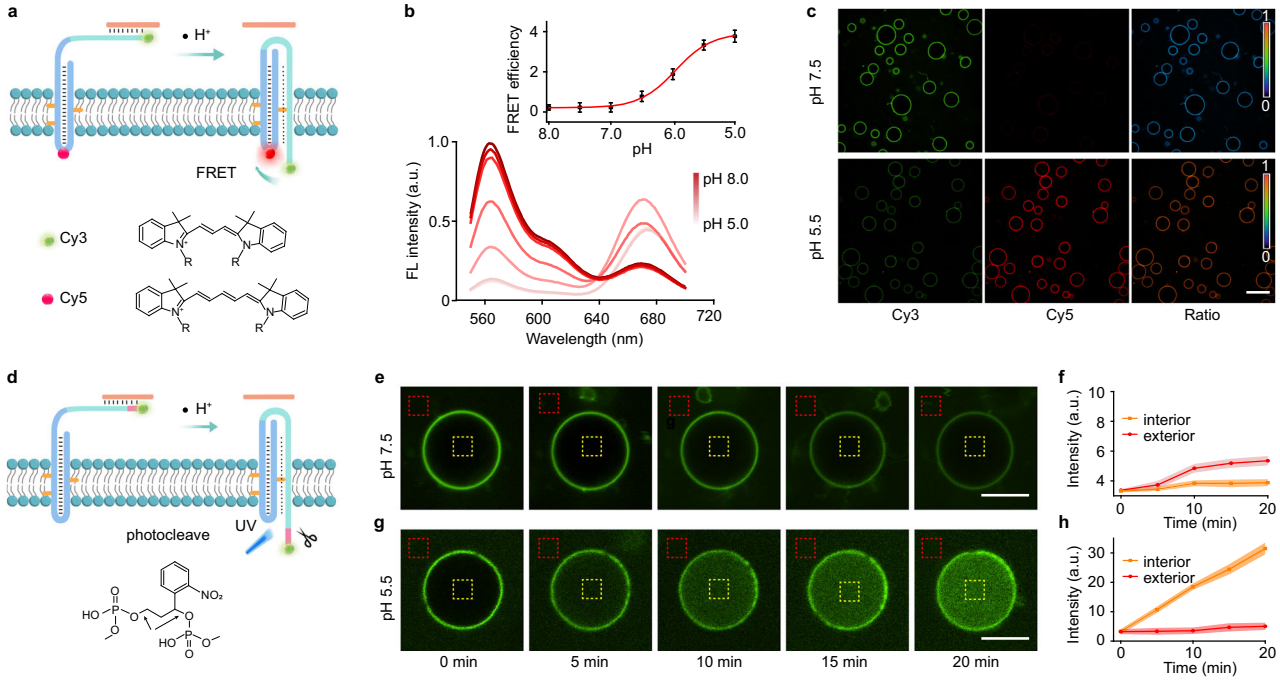

Fig. 4 | H⁺-mediated conformational change of TD receptors for transmembrane FRET and photocleavage. a Schematic diagram illustrating the pH-dependent conformational transition of the TD receptor, leading to FRET-based signal transduction. **b** Normalized fluorescence spectra showing increased FRET efficiency at 675 nm as the pH decreases from 8.0 to 5.0, indicating triplex formation. Inset: Quantitative analysis of the FRET efficiency (the Fa/Fd ratio, 675 nm to 570 nm). $Chol_3$-TD-FRET: 1 μM. Data are presented as mean ± s.d. ($n = 3$ independent samples). **c** Confocal fluorescence images of a single GUV showing strong Cy5 fluorescence at pH 5.5, confirming FRET occurrence due to triplex formation. **d** Schematic representation of the photocleavable linker (PC-linker) system used to validate transmembrane translocation of the signal module. **e**, **f** Fluorescence intensity changes in the exterior and interior of vesicles at high pH (7.5) upon UV irradiation, showing signal output remaining outside. **g**, **h** Fluorescence intensity changes in the exterior and interior of vesicles at low pH (5.5) upon UV irradiation, demonstrating signal translocation to the interior. Each experiment was independently repeated three times, with consistent results. Data in (**f**, **h**) are presented as mean ± s.d. ($n = 3$ independent GUVs). $Chol_3$-TD-PC-Cy3: 2 μM. Scale bars (**e**, **g**), 5 μm. a.u. arbitrary units.

cholesterol-tagged TD (Supplementary Fig. 17g–i), and the membrane of GUVs are impermeable to the small fluorescent DNA fragments (Supplementary Fig. 18).

Molecular dynamics simulations for the structural model of the synthetic receptor

The functionality of the TD-based synthetic receptor relies on the pH-induced conformational transition from duplex to triplex. To gain deeper insights into this process, we employed atomistic molecular dynamics (MD) simulations to investigate the interactions of the synthetic receptor with lipid bilayer membranes. The duplex and triplex conformations of the TD receptor are depicted in Fig. 5a, b, respectively. The cholesterol-tagged cholesterols located in the middle of the TD receptor interact with the hydrophobic region of the lipid bilayer, orienting the receptor perpendicularly to the membrane. Top-down views of the synthetic receptor in its two conformations are shown in Fig. 5c, d.

Simulations of the conformational dynamics of the TD receptor within the membrane were conducted over 100 ns for both conformations. Results indicated that both the duplex and triplex forms successfully integrate into the phospholipid membrane (Fig. 5e, f and Supplementary Fig. 19). The hydrophilic segments exposed on the membrane surface interact strongly with water molecules, contributing to the receptor's structural flexibility. This flexibility is quantified by per-residue root mean square fluctuation (RMSF) measurements (Supplementary Fig. 20), revealing that the duplex conformation exhibits greater flexibility compared to the triplex form. Correspondingly, the root mean square deviation (RMSD) values were higher for the duplex conformation (3.4 ± 0.1 nm) than for the triplex conformation (1.4 ± 0.1 nm) (Supplementary Fig. 21), reflecting its higher structural variability.

The greater structural flexibility of the duplex conformation is attributed to its extensive exposure to the aqueous environment. In addition, time-dependent binding energy calculations for the receptor in its two conformations demonstrated differential membrane interactions (Fig. 5g). The duplex conformation exhibited an average binding energy of $(-3.3 \pm 0.2) \times 10^3$ kJ/mol, whereas the triplex conformation showed a more favorable binding energy of $(-3.7 \pm 0.2) \times 10^3$ kJ/mol (Supplementary Fig. 22). These findings suggest that the spontaneous transition from duplex to triplex is energetically more favorable in the membrane environment, aligning with the observed structural dynamics and binding energies.

Pro-catalyst as a signal module for transmembrane fluorescence catalysis

Given that H⁺-ion-mediated triplex formation facilitates the translocation of the signal module from the membrane exterior to the interior, we further investigated triplex formation-mediated transmembrane fluorescence catalysis using a pro-catalyst-tagged signal module (Fig. 6a). The 5′-terminus of the TD was labeled with a dipyridylamine group (Supplementary Fig. 23) capable of coordinating with Zn^{2+} ions to catalyze the hydrolysis of carboxylate esters, such as the conversion of the low blue fluorescent substrate APTS into the green fluorescent product HPTS (Fig. 6b and Supplementary Fig. 24).

As shown in Fig. 6c, adding H⁺ to lower the external pH to 5.5 resulted in a dramatic increase in fluorescence (green line), with an 11-fold enhancement compared to the control without H⁺ addition (red line). The fluorescence enhancement was not due to H⁺ leakage into the vesicle, since no significant fluorescence emission was observed on the control without TDs-based artificial receptors over several hours at pH 5.5 (black line). The fluorescence signal amplification was strongly

https://doi.org/10.1038/s41467-024-53960-5

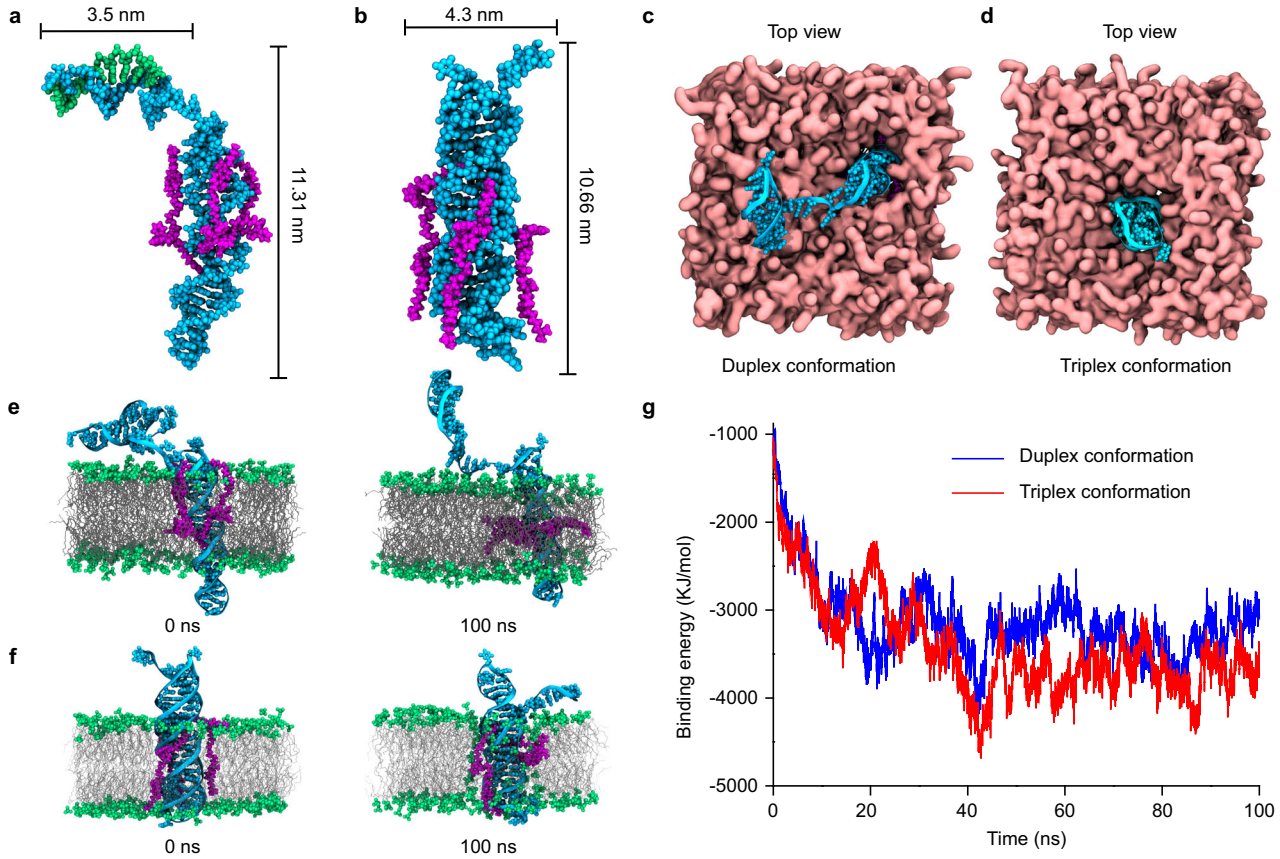

Fig. 5 | Molecular dynamics simulations of the TD-based synthetic receptor. Snapshot of the duplex conformation (**a**) or triplex conformation (**b**) of the TD receptor embedded in the lipid bilayer. Top-down views of the synthetic receptor in its duplex (**c**) and triplex (**d**) conformations. Side views showing the insertion of the duplex (**e**) and triplex (**f**) conformations into the lipid bilayer, MD simulation at 0 ns and 100 ns. **g** Time-dependent binding energy profiles for the duplex (blue) and triplex conformations (red) interacting with the lipid bilayer, indicating a more favorable binding energy for the triplex conformation.

dependent on the presence of immobilized TD and encapsulated APTS substrates (Fig. 6d, e). Increasing the amounts of TD and APTS substrates accelerated the fluorescence catalysis, indicating that external H^+ addition induces a conformational change in the artificial receptor, thereby activating the amine catalyst via coordination with zinc ions inside the vesicles.

The use of fluorescence catalysis for signal amplification was further explored through confocal imaging of individual GUVs (Fig. 6f–i). At an ambient pH of 7.5, the GUVs emitted no product fluorescence. However, upon lowering the external solution pH to 5.5 with H^+ addition, green HPTS fluorescence was observed inside the GUVs, indicating that the reaction occurred within the vesicles, as the substrate was encapsulated internally. The enhancement in HPTS fluorescence, along with the attenuation of APTS fluorescence in the blue window, confirmed the successful conversion of APTS to HPTS inside the vesicles. The transmembrane signal transduction was quantitatively assessed using flow cytometry (Fig. 6j–m). HPTS fluorescence steadily increased over 150 min, while the front scatter (FSC) and side scatter (SSC) intensities remained unchanged, indicating that the size and internal complexity of the GUVs were not affected during the acid-activated signal transduction process.

Synthetic receptor-based AND logic gates for signal transduction

The auxiliary sequence in the synthetic receptor system is a short oligonucleotide that is partly complementary to the third strand of the triplex DNA (TD). At low pH, the third strand preferentially forms a triplex with the duplex hairpin due to stronger Hoogsteen interactions, causing it to dissociate from the auxiliary sequence. However, increasing the length of the auxiliary sequence reinforces its binding to the third strand, preventing dissociation[37,38]. Theoretical calculations indicate that when the auxiliary sequence hybridizes with fewer than 14 bases of the third strand, the dissociation energy (ΔG_1) is lower than the binding energy (ΔG_2) required for triplex formation (Fig. 7a, b, and Supplementary Fig. 25). Verified in Fig. 7c, FRET efficiency decreases as the length of the auxiliary sequence increases. Conformational transformation conducive to FRET was highly probable with fewer than 14 nucleotides (nt) in the auxiliary sequence, while sequences longer than 14 nt significantly inhibited the FRET process. Confocal microscopy FRET ratio imaging confirmed that FRET was inactive when the auxiliary sequence length reached 16 nt (Supplementary Fig. 26).

To address the inhibition caused by longer auxiliary sequences ($n > 13$), we introduced a complementary DNA (cDNA) sequence as an entropy-driven input to displace the auxiliary sequence. Under this condition, we constructed an AND logic gate using the TD receptor to achieve dual input-controlled transmembrane signal transduction. The TD receptor was incorporated into GUVs, and its functionality was tested by introducing cDNA to displace the auxiliary sequence and H^+ to induce duplex-to-triplex conversion, thus activating the signal module (Fig. 7d). The FRET spectra (Fig. 7e) and confocal images (Fig. 7f and Supplementary Fig. 27) show that a distinct FRET output is produced in the vesicle only when both cDNA and H^+ are present. The absence of either input fails to generate a FRET signal, indicating that both inputs are required for successful signal transduction.

We extended this AND logic gate concept to the pro-catalyst-mediated transmembrane fluorescence catalysis (Fig. 7g). Fluorescence spectroscopy and optical imaging revealed that fluorescence enhancement occurred only when both cDNA and H^+ were present

https://doi.org/10.1038/s41467-024-53960-5

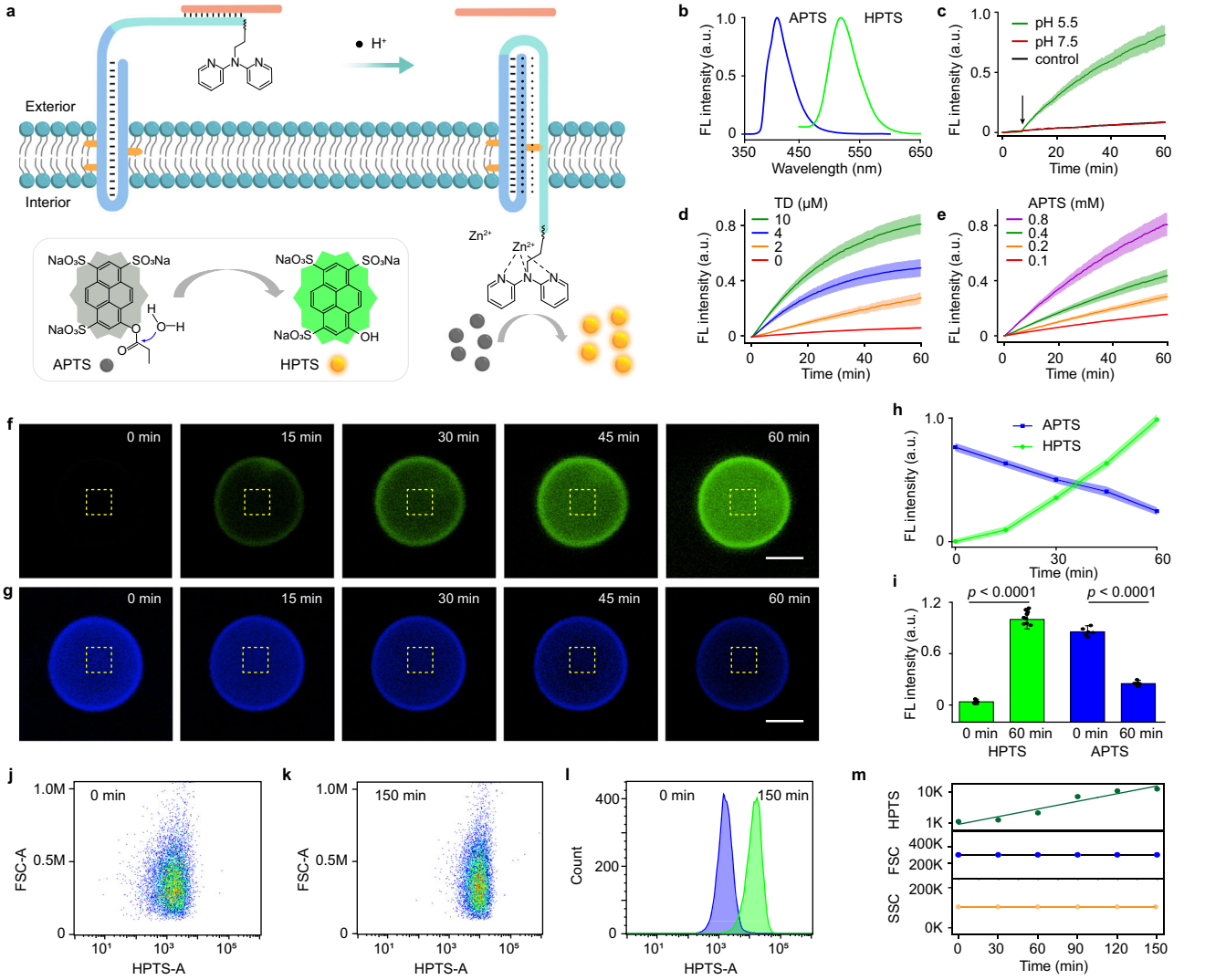

Fig. 6 | Pro-catalyst as a signal module for transmembrane fluorescence catalysis. a Schematic diagram of the pro-catalyst dipyridylamine used for transmembrane fluorescence catalysis. H^+-mediated triplex formation translocates the pro-catalyst dipyridylamine, tagged on the 5′-terminus of the TD, into the membrane interior in the presence of Zn^{2+}, where it catalyzes the conversion of APTS into HPTS. **b** Normalized fluorescence spectra of APTS (Em 390 nm) and HPTS (Em 520 nm). **c** Fluorescence kinetic profiles showing HPTS generation inside LUVs (Ex: 415 nm, Em: 510 nm) at an external pH of 7.5 (red line) and pH 5.5 after adding dilute HCl (aq) (green line), and control vesicles without TD incubated at an external pH of 5.5 (black line). APTS, 250 μM; Zn^{2+}, 250 μM; TD, 10 μM; Aux_{11}, 50 μM; 1 mM DOPC lipid. Fluorescence kinetic curves showing dependency on TD concentration (**d**) and APTS substrate concentration (**e**). TD: 0-10 μM; APTS: 0.1–1 mM; TD = 1:5 molar ratio. Data in (**c**–**e**) are presented as mean ± s.d. ($n = 3$ independent samples). **f**–**i** Time-dependent confocal fluorescence imaging illustrating HPTS fluorescence enhancement over time (**f**) with concurrent attenuation of APTS fluorescence (**g**). Quantitative intensity analysis (**h**) and fluorescence intensity histogram comparison at 0 and 60 min (**i**). Data in (**h**, **i**) are presented as mean ± s.d., ($n = 3$ independent GUVs in **h**, and $n = 6$ independent GUVs in **i**, two-sided Student's t-test); Scale bar (**f**, **g**), 5.0 μm. Two-dimensional flow cytometry scatter plots of FSC-A versus HPTS-A, showing signal transduction at t = 0 (**j**) and t = 150 min (**k**), with a corresponding histogram of HPTS fluorescence (**l**). **m** Time-dependent changes in mean HPTS fluorescence (green), mean FSC intensity (blue), and mean SSC intensity (yellow) within vesicles. a.u. arbitrary units.

(Fig. 7h, i). This demonstrates that the substitution of the auxiliary sequence by cDNA (input 1) and the subsequent addition of H^+ (input 2) are necessary to activate the TD receptor's conformational transformation, leading to effective transmembrane fluorescence signaling.

Discussion

This study established a system for artificial transmembrane signal transduction by leveraging the stimuli-responsive conformational transition of triplex DNA (TD) to facilitate intracellular and extracellular communication. Cholesterol groups attached to the middle of the TD sequences provided an anchor for the perpendicular immobilization of the synthetic receptor on lipid bilayer membranes. An auxiliary sequence complementary to the third strand of the TD served as a steric hindrance module, ensuring a preferred orientation towards the outer leaflet. The low pH-induced transition of TD from a duplex to a triplex conformation, coupled with the translocation of the third strand from the membrane's outer leaflet to the inner leaflet, was validated through FRET and selective photocleavage experiments. Fluorescence signal amplification was further achieved within the vesicle interior when the signal module was replaced with a pro-catalyst. Additionally, logic gate signal transduction was demonstrated by modifying the number of nucleotides in the auxiliary sequence, enabling the application of the synthetic receptor in logic circuits.

This work presents a versatile design for synthetic receptors characterized by modularity, programmability, and controllability. It demonstrated that conformational change is an effective mechanism for transmembrane signal transduction in synthetic systems, integrating oriented membrane immobilization, stimulus response, and

https://doi.org/10.1038/s41467-024-53960-5

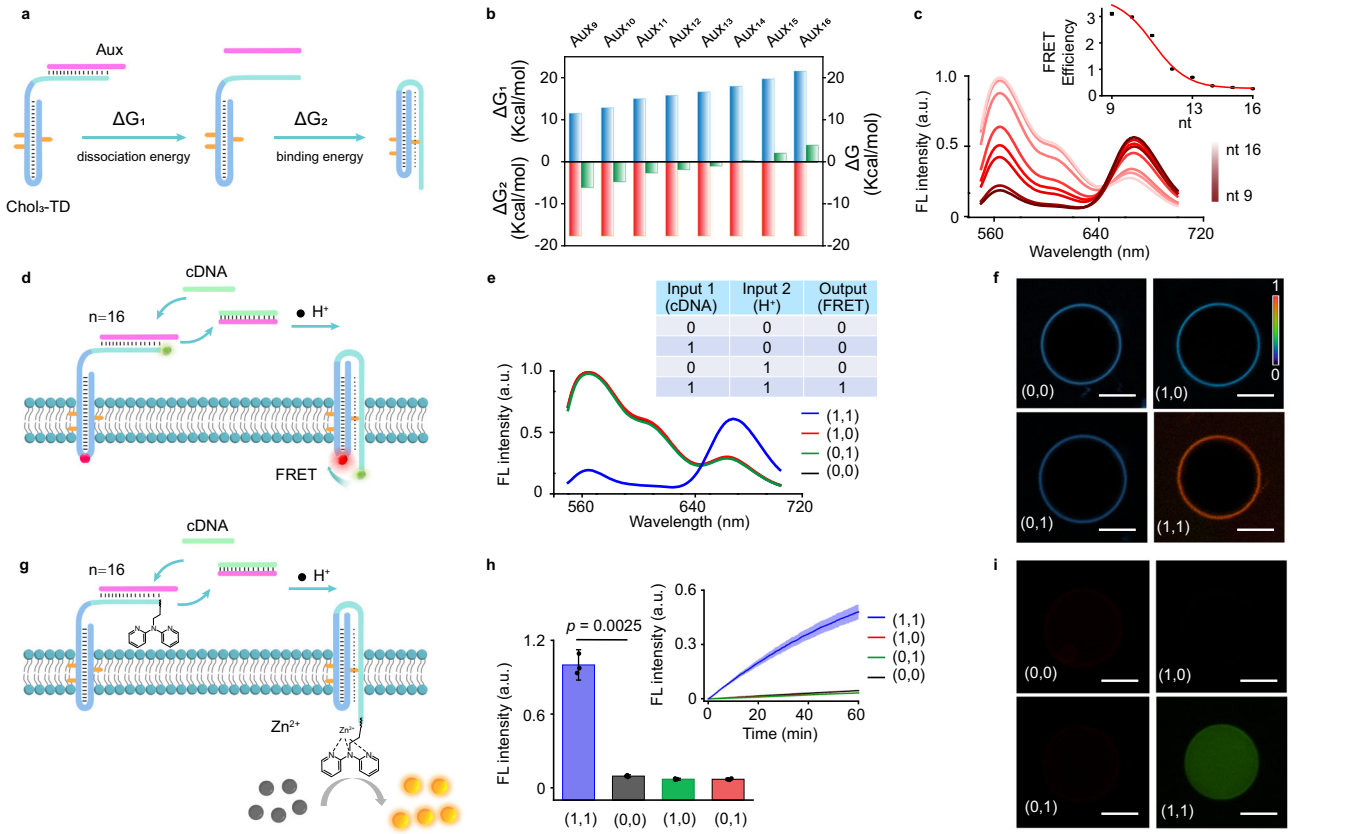

Fig. 7 | Synthetic receptor-based AND logic gates for signal transduction. **a** Schematic diagram illustrating the state transition of $Chol_3$-TD. **b** Dissociation energy (ΔG_1) of $Chol_3$-TD with different complementary auxiliary strands Aux_n ($n = 9–16$) and binding energy (ΔG_2) for the triplex conformation, where $\Delta G = \Delta G_1 + \Delta G_2$. **c** FRET emission plot showing the H^+-mediated conformational change of the synthetic receptor in the presence of Aux_n ($n = 9–16$) at pH 5.5, monitored through a pH-insensitive FRET pair (Cy3/Cy5). Inset: FRET efficiency as a function of auxiliary sequence length. Increased nucleotide count of the auxiliary sequence inhibits the conformational transformation required for the FRET process. Data are presented as mean ± s.d. ($n = 3$ independent samples). **d** Design of AND logic gates for FRET signal transduction systems using Aux_{16}. cDNA (input 1) and H^+ (input 2) were used as dual inputs to initiate transmembrane FRET (output). cDNA, 5.0 μM; H^+ ions, pH 5.5. **e** FRET fluorescence spectroscopy under different conditions. Inset: Truth table for AND logic gates. A significant FRET output signal was detected only with the simultaneous presence of both input 1 and input 2. **f** Confocal fluorescence ratio images of GUVs under different conditions showing FRET signal dependent on dual input activation. Each experiment was independently repeated three times, with consistent results. **g** Design of AND logic gates for fluorescence catalytic signal transduction systems using Aux_{16}. cDNA and H^+ were used as dual inputs to initiate transmembrane fluorescence catalysis. cDNA, 50 μM; H^+ ions, pH 5.5. **h** Fluorescence histogram under different conditions. Inset: Time-dependent fluorescence curve. The fluorescence catalytic signal was observed only with the simultaneous presence of both input 1 and input 2. Data in (**h**) are presented as mean ± s.d., two-sided Student's t-test ($n = 3$ independent experiments). **i** Confocal fluorescence ratio images of GUVs under different conditions, showing fluorescence signals dependent on dual input activation. Each experiment was independently repeated three times, with consistent results. Scale bar (**f**–**i**), 5.0 μm. a.u. arbitrary units.

conformational transformation combined with catalyst activation within vesicles. Although TD-based synthetic receptors are structurally and functionally simpler than natural G protein-coupled receptors (GPCRs), they exhibit essential features required for minimal synthetic receptors. This synthetic approach offers potential for designing a new class of chemical tools capable of controlling native cellular activities. Consequently, this research paves the way for developing vesicles sensitive to various chemical cues, ultimately laying the groundwork for bioinspired nanotechnologies that can interact with and exchange information with biological systems.

Methods

Materials

All reagents and solvents for synthesis were purchased commercially and used without further purification. 1,2-dipalmitoyl-*sn*-glycero-3-phosphocholine (DPPC), 1,2-Dioleoyl-sn-glycero-3-phosphocholine (DOPC) and Egg-yolk phosphatidylcholine (EYPC) were purchased from Avanti. Oleic acid, cholesterol and 8-aminopyrene-1,3,6-triasulfonic acid trisodium salt (APTS, ≥95%) and 8-Hydroxypyrene-1,3,6-trisulfonic acid (HPTS, ≥98%), Cholesterol-TEG-N_3 was obtained from Sigma-Aldrich. (2,2′-bipyridyl) thioethylamine was obtained from J&K Scientific (≥98%). Zinc chloride, Tris and (N-2-hydroxyethylpiperazine-N-2-ethane sulfonic acid) HEPES were purchased from Sinopharm. DNase 1 was purchased from Sangon Biotech (1 KU/mL). Milli-Q-purified water (18.2 MΩ cm) was used for all the experiments.

Synthesis of cholesterol-tagged triplex DNA (TD)

DBCO-modified triplex-forming oligonucleotides (TD), including $DBCO_1$-TD, $DBCO_2$-TD, $DBCO_3$-TD, $DBCO_3$-TD-Cy3, $DBCO_3$-TD-PC-Cy3, $DBCO_3$-TD-FRET, $DBCO_3$-TD-Malei (Table S1), were synthesized by solid-phase phosphoramidite chemistry and purified using high-performance liquid chromatography (HPLC) in Sango Biotech. The cholesterol-tagged TD were prepared through click reaction of DBCO-modified TD with azide-functionalized cholesterol (Cholesterol-TEG-N_3) (Figure S1). 300 μM Cholesterol-TEG-N_3 were incubated overnight with 100 μM DBCO-modified TD in (methanol: acetonitrile: H_2O_2 = 1:1:1) at 45 °C. The synthesized cholesterol-tagged TD ($Chol_1$-TD, $Chol_2$-TD, $Chol_3$-TD, $Chol_3$-TD-Cy3, $Chol_3$-TD-PC-Cy3, $Chol_3$-TD-FRET, $Chol_3$-TD-Malei (Table S1)) were characterized by electrospray ionization-mass spectrometry (ESI-MS) and purified using high-

performance liquid chromatography (HPLC). The yield is more than 95%.

Preparation of large unilamellar vesicles (LUVs)

LUVs were prepared using a lipid film hydration method in a 100 mM HEPES buffer(pH 7.5). To a round bottom flask was added 1 mL chloroform/methanol solutions of the lipids DPPC (or DOPC) and cholesterol, in a 9:1 molar ratio, (small amount of oleic acid), in order to obtain final concentrations of 1 mM for the lipids. The solvent was removed from the rotary evaporator and dried under high vacuum for 2 h. A 100 mM solution of HEPES buffer at pH 7.5 (1 mL) was added to the flask containing the lipids, and sonicated for 10 min. The suspension was subjected to 5 cycles of freeze-thaw using liquid nitrogen. The suspension was extruded for 19 times through a polycarbonate filter with 200 nm pores in an Avanti Mini Extruder apparatus, and then the vesicles were separated by the bulk solution using prepacked NAP-10 (GE Healthcare) columns eluting with a 100 mM HEPES solution at pH 7.5.

Preparation of giant unilamellar vesicles (GUVs)

GUVs were prepared by electro formation technique. In total, 10 μL of a 10 mM solution of EYPC and cholesterol (9:1 in molar) in chloroform was spread evenly on the indium tin oxide (ITO)-coated glass slides within the "O" ring area. The solvent was evaporated at room temperature, and the slides were dried overnight under vacuum. Then, ITO slides were assembled and filled with 300 μL of buffer (100 mM HEPES, pH 7.5). A sinusoidal AC field of 3 V and 5 Hz was applied for 2 h at 25 °C temperature. The GUVs solution prepared was collected and stored at 4 °C. The concentration of the GUVs stock solution was determined at around 10^5 number/mL.

The orientation of cholesterol-tagged TD on the membranes

Linear dichroism. Linear dichroism (LD) is a method to study molecular orientation. It is based on the preferential absorption of polarized light oriented in the same direction as the electric transition dipole moment of a given chromophore. Structural information may be obtained from LD about how the molecule is oriented with respect to the polarization of the incident light. Solution-phase flow linear dichroism (LD) spectroscopy was performed on a Biologic MOS-500 (Bio-Logic) using a photo elastic modulator 1/2 wave plate. A micro-volume quartz Couette flow cell with ~0.5 mm annular gap and quartz capillaries were used. Molecular alignment was achieved by applying the constant flow of the sample solution between two coaxial cylinders, a stationary quartz rod and a rotating cylindrical capillary. LD spectra were determined after TD sequences (TD, $Chol_1$-TD, $Chol_2$-TD, $Chol_3$-TD) at 2 μM were incubated with LUVs (500 μM DOPC, 100 mM HEPES, sucrose 50% w/w, pH 7.5) for 10 min.

Enzyme digestion assay. A solution of the lipid DOPC (100 μL, 10 mM) in chloroform was added to a 1 mL round bottom flask. The solvent was removed using a rotary evaporator (IKA, Germany) to yield a thin film. The lipid was re-suspended in 100 mM Tris buffer (25 mM $MgCl_2$, 1 mM $CaCl_2$, pH 7.5), sonicated for 20 min at 30 °C and then equilibrated for 3 h. For assays with vesicles, cholesterol-tagged TD sequences $Chol_3$-TD-Cy3 hybridize with and without auxiliary strand Aux_{11} (2 μL, 50 μM) were first incubated with LUVs (19 μL, 1 mM DOPC) for 1 h then added to the 10 mm quartz cuvette with 80 μL buffer. Cy3 was selected due to its environment-sensitive properties which lead to significant fluorescence changes depending on the dye's attachment to a duplex, single-strand, isolated nucleotides, or in a free-dye state. Therefore, the orientation of $Chol_3$-TD-Cy3 was quantified by changes in Cy3 fluorescence, and when 5′-Cy3 is oriented outward toward the membrane, the exposed portion of the $Chol_3$-TD-Cy3 is rapidly degraded by DNase 1 and the fluorescence decreases, whereas the portion that is oriented inward is protected from enzyme degradation due to the protection of the lipid bilayer membrane. The change in fluorescence induced by the addition of Triton-100 to cause vesicle cleavage followed by the addition of DNase 1 served as a baseline for quantification. Fluorescence was monitored using a F7000 fluorescence spectrophotometer (Hitachi) at 570 nm and excited at 555 nm. After 5 min, nuclease DNase 1 (1 μL, 1 KU/mL, Sangon Biotech) was added, and the fluorescence emission was monitored for 10 min. In the control group, the above samples were added with 2 μL 1% Triton-100 to lyse the vesicles, and then the fluorescence changes were monitored after the addition of DNase1. Their fluorescence would reach a platform in 10 min, and the fluorescence platform serves as a baseline (dotted line in Fig. 2b, e) that all the DNA sequences in the control group are completely digested by DNase 1.

Fluorescence recovery assay. The Cy3-labeled TD ($Chol_3$-TD-Cy3) and the auxiliary strand BHQ2-Aux_{11} (labeled with BHQ2) were annealed and assembled in 100 mM HEPES (pH 7.5). The DNA receptors (100 nM, $Chol_3$-TD-Cy3: BHQ2-Aux_{11} = 1: 5) were then incubated with LUVs (1 mM for the lipids, pH 7.5) for half an hour and centrifuged to remove free DNA receptors. The change in fluorescence was then monitored after the addition of the $cDNA_{11}$ sequence (500 nM), which replaced the auxiliary strand BHQ2-Aux_{11} to restore the fluorescence of the $Chol_3$-TD-Cy3. In the control group, the above samples were added with 2 μL 1% Triton-100 to lyse the vesicles, and then the fluorescence changes were monitored after the addition of $cDNA_{11}$. The excitation wavelength was 540 nm and the emission spectrum was monitored at 575 nm or scanned between 550 and 650 nm. Their fluorescence in the control group would reach a plaTDrm, which serves as a baseline that all the BHQ2-Aux_{11} sequences in the control group are completely replaced by $cDNA_{11}$ strand.

Conformation changes of cholesterol-tagged TD in solution characterized by FRET and CD spectra

500 nM cholesterol-tagged FRET TD ($Chol_3$-TD-FRET) in the presence of 2 μM auxiliary sequence (Aux_{11}) was incubated in Tris buffer at different pH values (pH = 4.5, 5.0, 5.5, 6.0, 6.5, 7.0, 7.5, 8.0) for 1 h, and then scanned in the NIR steady-state fluorescence spectrometer (Ex: 530 nm, Em: 550–700 nm). Meanwhile, circular dichroism (CD) spectra of the cholesterol-tagged TD ($Chol_3$-TD) were measured at a pH gradient of 4.5, 5.0, 5.5, 6.0, 6.5, 7.0, 7.5, and 8.0. Circular dichroism spectroscopy was performed on a MOS-500 (Bio-Logic) scanning in the range of 200-320 nm. A micro-volume quartz Cuvette flow cell with ~0.5 mm annular gap and quartz capillaries were used (Kromatec Ltd, Great Dunmow, UK). The final concentration of the $Chol_3$-TD was 5 μM, the final volume of the samples was 200 μL, and the average value was determined by taking three measurements for each sample.

Molecular dynamics simulations

The atomic model of cholesterol-tagged TD in duplex state at high pH value and triplex state at low-pH value were simulated in caDNAno, then converted to all atom models in python according to the experimental nucleotide sequence. Three-dimensional structures of TD at duplex and triplex conformations were constructed separately, and TEG-cholesterol was modified at three different T base sites. The modified structure is first subjected to energy optimization by using the Amber14SB force field. The optimization process is carried out in two steps: first, the 2000-step steepest descent method is used to optimize, and then the 2000-step conjugate gradient method is used to further optimize the structure, the final result as a model for subsequent research. Following that, the structure of phospholipid cell membranes consists of 294 pre-equilibrated 1,2-Dioleoyl-sn-glycero-3-phosphocholine (DOPC) molecules. First, the structure of the phospholipid membrane was constructed using CHARMM-GUI. The size of the box was 10 nm × 10 nm × 8.5 nm, filled with water molecules and counter ions, and a 20 ns equilibrium simulation was performed by using Amber14SB atomistic force field implemented in GROMACS simulation packages, under constant temperature and pressure and

periodic boundary conditions, and the box size was stabilized at 9.68 nm ×9.68 nm × 8.05 nm.

The cholesterol-tagged TD were inserted into the patch of lipid bilayer membrane such that the TD were inside the hydrophobic region of the bilayer. For simulations of membrane tethered cholesterol-tagged TD, VMD was used to generate the membranes and orient the TD nanostructures while maintaining favorable cholesterol orientations. The membrane-spanning cholesterol-tagged TD were simulated in a 10 nm × 10 nm × 8.5 nm box of 1 M KCl and TIP3 water prepared in VMD, duplex TD were simulated in 10 nm × 10 nm × 8.5 nm box and triplex TD were simulated in a box of 10 nm × 10 nm × 8.5 nm box.

In the MD simulation process, all involved hydrogen bonds are constrained by the LINCS algorithm, and the integration step size is 2 fs. Electrostatic interactions were calculated using the (Particle-mesh Ewald) PME method. The non-bonded interaction cutoff was set to 10 Å and updated every 10 steps. The simulated temperature was controlled to 300 K using the V-rescale temperature coupling method, and the pressure was controlled to 1 bar using the Parrinello-Rahman method. First, the energy minimization of the two systems was carried out using the steepest descent method to eliminate too close contacts between the atoms; then, the NVT equilibrium simulation was performed at 300 K for 100 ps; finally, the MD of the two systems was performed for 100 ns respectively, conformations were saved every 10 ps, and the visualization of the simulation results was done using the Gromacs embedded program and VMD. It is likely that the DNA nanostructures anchored by hydrophobic tags would form a toroidal pore in the membrane and changes the structure of the membrane.

RMSF: gmx_covar and gmx_aneig were used to investigate the ten top quasi-harmonic modes of root mean squared fluctuations (RMSF) of the DNA backbone heavy atoms, averaged per-residue, to interrogate structural dynamics of the cholesterol-tagged TD while accounting for thermal noise and stochastic motion.

Transmembrane signal transduction-mediated fluorescence resonance energy transfer (FRET)

A FRET assay based on Cy3, Cy5-labelled and three cholesterol-tagged TD ($Chol_3$-TD-FRET) in the presence of auxiliary sequence (Aux_{11}) were used to confirm the H^+-mediated triplex formation and signal transductions. Cholesterol-tagged TD ($Chol_3$-TD-FRET) (1 μM) with auxiliary sequence Aux_{11} (5 μM) were added to vesicle solution (LUVs: 1 mM for the lipids, OR GUVs: about 300 μM for the lipids). Adding small aliquots of dilute $HCl_{(aq)}$ to the vesicle solution reduced its pH from 7.5 to 5.5, which initiated the $Chol_3$-TD-FRET conformation transformation from duplex to triplex and subsequent occurrence of FRET. Near-infrared steady-state fluorescence spectroscopy (Ex: 530 nm, Em: 550–700 nm) and confocal fluorescence microscopy were used to characterize the transmembrane FRET signal.

Transmembrane signal transductions-mediated intravesicular photocleavage experiments

A photocleavage experiment based on ($Chol_3$-TD-PC-Cy3) in the presence of auxiliary sequence (Aux_{11}) were conducted to confirm the conformation change-mediated transmembrane signal transduction. A photocleavage group of PC-linker and fluorescence Cy3 were attached to 5′-terminals of the $Chol_3$-TD-PC-Cy3. The PC-linker group can be broken up under ultraviolet light irradiation, and the terminal Cy3 would fall off from the TD sequences. Incubation of 2 μM photocleavage TD ($Chol_3$-TD-PC-Cy3) in the presence of 10 μM Aux_{11} in the suspension of GUVs (300 μM lipids) at pH 7.5 for half an hour. Then small aliquots of dilute $HCl_{(aq)}$ was added to the sample to make the pH of the system change to 5.5, then irradiated it with 350 nm ultraviolet light for 20 min. The fluorescence changes inside and outside the vesicles were monitored. As a control experiment, the UV light irradiation was conducted before and after the addition of small aliquots of dilute $HCl_{(aq)}$. The fluorescent imaging of the vesicles was conducted via fluorescent confocal microscopy (Ex: 561 nm, Em: 570–620 nm).

Transmembrane signal transductions for metal hydrolase reaction

Triplex DNA-mediated transmembrane signal transduction would initiate a fluorescence signal amplification if the 5′ terminal of cholesterol-tagged TD was labelled with (2, 2′-bipyridyl) thioethylamine (BPEA) group, which can bind with Zn^{2+} for catalyzing the conversion of the non-fluorescent ester substrate 8-acetoxypyrene-1,3,6-trisulfonatetrisodium salt (APTS), into a fluorescent output signal, namely, 8-hydroxypyrene-1,3,6-trisulfonatetrisodium salt (HPTS). BPEA-tagged $Chol_3$-TD ($Chol_3$-TD-BPEA) were prepared through mix of 100 μM Cholesterol-tagged maleimide group activated TD ($Chol_3$-TD-Malei) with excessive (2, 2′-bipyridyl) thioethylamine, and adjust the pH value from 6.5 to 7.5. The maleimide group will react specifically with the sulfhydryl group of (2, 2′-bipyridyl) thioethylamine to form an irreversible stable thioether bond. After shaking overnight at 37 °C, the product of BPEA-tagged TD ($Chol_3$-TD-BPEA) were obtained after dialysis to remove the unreacted small molecule. The molecular weight of the product was analyzed by electrospray ionization-mass spectrometry.

BPEA-tagged $Chol_3$-TD ($Chol_3$-TD-BPEA) (10 μM) in the presence of Aux_{11} (50 μM) were added to a suspension of vesicles (LUVs: 1 mM for the lipids, OR GUVs: about 300 μM for the lipids, 100 mM HEPES) loading with Zn^{2+} (250 μM) and APTS (250 μM). Small aliquots of dilute $HCl_{(aq)}$ were added to the vesicle solution to reduce its pH from 7.5 to 5.5, which initiated the $Chol_3$-TD-BPEA transformation from duplex to triplex and consequently translocation of the BPEA catalyst group from the membrane exterior into the membrane interior. BPEA in the 5′ terminal of the $Chol_3$-TD-BPEA binding with Zn^{2+} and catalyze the non-fluorescent APTS into HPTS. Steady-state fluorescence spectroscopy (Ex: 415 nm, Em: 440–650 nm) was used to characterize the fluorescence signal. Meanwhile, fluorescence excitation spectra were recorded using the following parameters: Em: 488 nm, Ex: 500–550 nm, recorded at 2 minutes intervals. Confocal fluorescence microscopy imaging was performed on a TI-E + A1 SI Nikon confocal laser scanning microscope. All fluorophores were imaged using sequential scanning. HPTS was excited using a 65 mW Ar laser (Ex: 488 nm, Em: 500–550 nm, 35% power); APTS was excited at 405 nm and fluorescence emission collected in the 425–475 nm; Cy3 was excited at 561 nm and fluorescence emission collected in the 570–620 nm; Cy5 was excited 20 mW helium–neon gas laser (Ex: 640 nm, Em: 663–738 nm, 35% power).

AND logic gate for transmembrane signal transductions

Cy3, Cy5-tagged cholesterol-tagged TD ($Chol_3$-TD-FRET) (1 μM) in the presence of Aux_n (n = 9, 10, 11, 12, 13, 14, 15, 16) (5 μM) were added to a suspension of vesicles (LUVs: 1 mM for the lipids, OR GUVs: about 300 μM for the lipids). Adding small aliquots of dilute $HCl_{(aq)}$ to the vesicle solution reduced its pH from 7.5 to 5.5, which initiated the $Chol_3$-TD-FRET conformation transformation from duplex to triplex and subsequent occurrence of FRET. Near-infrared steady-state fluorescence spectroscopy (Ex: 530 nm, Em: 550–700 nm) and confocal fluorescence microscopy were used to characterize the transmembrane FRET signal. ($Chol_3$-TD-FRET) (1 μM) in the presence of Aux_{16} (5 μM) were added to a suspension of vesicles (GUVs: about 300 μM for the lipids). Either small aliquots of dilute $HCl_{(aq)}$ were added to the vesicle solution reduced its pH from 7.5 to 5.5, or added only to $cDNA_{16}$ (5 μM), or both to the vesicle solution, then characterized by confocal fluorescence microscopy for the transmembrane FRET signaling.

BPEA-tagged cholesterol-tagged TD ($Chol_3$-TD-BPEA) (10 μM) in the presence of Aux_{16} (50 μM) were added to a suspension of vesicles (LUVs: 1 mM for the lipids, OR GUVs: about 300 μM for the lipids)

loading with Zn^{2+} (250 μM) and APTS (250 μM). Adding small aliquots of dilute $HCl_{(aq)}$ to the vesicle solution reduced its pH from 7.5 to 5.5, or only adding $cDNA_{16}$ (50 μM), or both to the vesicle solution, then characterized by both fluorescence spectroscopy (Em: 488 nm, Ex: 500–550 nm) and confocal fluorescence microscopy for the transmembrane fluorescence signal.

Statistics and reproducibility

Statistical parameters, including the definitions and exact values of n (for example, number of experiments, number of GUVs, and so on), distributions and deviations are reported in the figures and corresponding figure legends. All experiments were repeated at least three times and all data are expressed as mean ± s.d. Statistical analyzes were performed using Origin 2018. Two-sided unpaired Student's t-tests were used for comparison between two groups according to data distribution. Values were normally distributed and the variance was similar between compared groups. $P < 0.05$ was considered statistically significant.

Reporting summary

Further information on research design is available in the Nature Portfolio Reporting Summary linked to this article.

Data availability

The authors declare that the data supporting the findings of this study are available within the paper and its Supplementary Information files. Source data are provided with this paper. The source data underlying Figs. 2c–f, 3b, c, e, f, h, j, 4b–c, e–h, 5g, 6b–m and 6b, c, e, f, h, i are provided as a Source Data file. The source data are available from figshare, visit https://doi.org/10.6084/m9.figshare.26759929. Additional data are available from the corresponding author upon reasonable request.

References

1. Krauss, G. *Biochemistry of Signal Transduction and Regulation* 3rd edn, (Wiley, 2006).
2. Simon, M. I., Strathmann, M. P. & Gautam, N. Diversity of G proteins in signal transduction. *Science* **252**, 802–808 (1991).
3. Shen, J., Ren, C. & Zeng, H. Membrane-active molecular machines. *Acc. Chem. Res.* **55**, 1148–1159 (2022).
4. Li, H. et al. Efficient, non-toxic anion transport by synthetic carriers in cells and epithelia. *Nat. Chem.* **8**, 24–32 (2016).
5. Li, H. et al. Artificial receptor-mediated phototransduction toward protocellular subcompartmentalization and signaling encoded logic gates. *Sci. Adv.* **9**, eade5853 (2023).
6. Lemmon, M. A. & Schlessinger, J. Cell signaling by receptor tyrosine kinases. *Cell* **103**, 211–225 (2000).
7. Dorsam, R. T. & Gutkind, J. S. G-protein-coupled receptors and cancer. *Nat. Rev. Cancer* **7**, 79–94 (2007).
8. Shi, K., Song, C., Wang, Y., Chandrawati, R. & Lin, Y. Engineering receptor-mediated transmembrane signaling in artificial and living cells. *Commun. Mater.* **4**, 65 (2023).
9. Barton, P., Hunter, C. A., Potter, T. J., Webb, S. J. & Williams, N. H. Transmembrane signalling. *Angew. Chem. Int. Ed.* **41**, 3878–3881 (2002).
10. Dijkstra, H. P. et al. Transmission of binding information across lipid bilayers. *Chem. Eur. J.* **13**, 7215–7222 (2007).
11. Bernitzki, K. & Schrader, T. Entirely artificial signal transduction with a primary messenger. *Angew. Chem. Int. Ed.* **48**, 8001–8005 (2009).
12. Chen, H. et al. DNA-based artificial receptors as transmembrane signal transduction systems for protocellular communication. *Angew. Chem. Int. Ed.* **62**, e202301559 (2023).
13. Chen, H. et al. Controlled dimerization of artificial membrane receptors for transmembrane signal transduction. *Chem. Sci.* **12**, 8224–8230 (2021).
14. Brioche, J. et al. Conformational switching of a foldamer in a multicomponent system by pH-filtered selection between competing noncovalent interactions. *J. Am. Chem. Soc.* **137**, 6680–6691 (2015).
15. Eccles, N. et al. Remote conformational responses to enantiomeric excess in carboxylate-binding dynamic foldamers. *Chem. Commun.* **55**, 9331–9334 (2019).
16. De Poli, M. et al. Conformational photoswitching of a synthetic peptide foldamer bound within a phospholipid bilayer. *Science* **352**, 575–580 (2016).
17. Lister, F. G. A., Le Bailly, B. A. F., Webb, S. J. & Clayden, J. Ligand modulated conformational switching in a fully synthetic membrane-bound receptor. *Nat. Chem.* **9**, 420–425 (2017).
18. Langton, M. J., Keymeulen, F., Ciaccia, M., Williams, N. H. & Hunter, C. A. Controlled membrane translocation provides a mechanism for signal transduction and amplification. *Nat. Chem.* **9**, 426–430 (2017).
19. Langton, M. J., Scriven, L. M., Williams, N. H. & Hunter, C. A. Triggered release from lipid bilayer vesicles by an artificial transmembrane signal transduction system. *J. Am. Chem. Soc.* **139**, 15768–15773 (2017).
20. Langton, M. J., Williams, N. H. & Hunter, C. A. Recognition-controlled membrane translocation for signal transduction across lipid bilayers. *J. Am. Chem. Soc.* **139**, 6461–6466 (2017).
21. Ding, Y., Williams, N. H. & Hunter, C. A. A synthetic vesicle-to-vesicle communication system. *J. Am. Chem. Soc.* **141**, 17847–17853 (2019).
22. Langecker, M. et al. Synthetic lipid membrane channels formed by designed DNA nanostructures. *Science* **338**, 932–936 (2012).
23. Burns, J. R., Al-Juffali, N., Janes, S. M. & Howorka, S. Membrane-spanning DNA nanopores with cytotoxic effect. *Angew. Chem. Int. Ed.* **53**, 12466–12470 (2014).
24. Seifert, A. et al. Bilayer-spanning DNA nanopores with voltage-switching between open and closed state. *ACS Nano* **9**, 1117–1126 (2015).
25. Debnath, M. et al. Ionophore constructed from non-covalent assembly of a G-quadruplex and liponucleoside transports K^+-ion across biological membranes. *Nat. Commun.* **11**, 469 (2020).
26. Birkholz, O. et al. Multi-functional DNA nanostructures that puncture and remodel lipid membranes into hybrid materials. *Nat. Commun.* **9**, 1521 (2018).
27. Blanchard, A. T. & Salaita, K. Emerging uses of DNA mechanical devices. *Science* **365**, 1080–1081 (2019).
28. Li, C. et al. Triplex-forming oligonucleotides as an anti-gene technique for cancer therapy. *Front. Pharmacol.* **13**, 1007723 (2022).
29. Idili, A., Vallée-Bélisle, A. & Ricci, F. Programmable pH-triggered DNA nanoswitches. *J. Am. Chem. Soc.* **136**, 5836–5839 (2014).
30. Hu, Y., Cecconello, A., Idili, A., Ricci, F. & Willner, I. Triplex DNA nanostructures: from basic properties to applications. *Angew. Chem. Int. Ed.* **56**, 15210–15233 (2017).
31. Zheng, J. et al. Logic-gated proximity aptasensing for cell-surface real-time monitoring of apoptosis. *Angew. Chem. Int. Ed.* **60**, 20858–20864 (2021).
32. Banchelli, M. et al. Phospholipid membranes decorated by cholesterol-based oligonucleotides as soft hybrid nanostructures. *J. Phys. Chem. B* **112**, 10942–10952 (2008).
33. Lundberg, E. P., Feng, B., Mohammadi, A. S., Wilhelmsson, L. M. & Nordén, B. Controlling and monitoring orientation of DNA nanoconstructs on lipid surfaces. *Langmuir* **29**, 285–293 (2013).
34. Chen, S. et al. Systematic interrogation of cellular signaling in live cells using a membrane-anchored DNA multitasking processor. *Angew. Chem. Int. Ed.* **61**, e202113795 (2022).

35. Burns, J. R. & Howorka, S. Defined bilayer interactions of DNA nanopores revealed with a nuclease-based nanoprobe strategy. *ACS Nano* **12**, 3263–3271 (2018).
36. Lanphere, C. et al. Triggered assembly of a DNA-based membrane channel. *J. Am. Chem. Soc.* **144**, 4333–4344 (2022).
37. Porchetta, A., Idili, A., Vallée-Bélisle, A. & Ricci, F. General strategy to introduce pH-induced allostery in DNA-based receptors to achieve controlled release of ligands. *Nano Lett.* **15**, 4467–4471 (2015).
38. Amodio, A., Adedeji, A. F., Castronovo, M., Franco, E. & Ricci, F. pH-controlled assembly of DNA tiles. *J. Am. Chem. Soc.* **138**, 12735–12738 (2016).

Acknowledgements

The authors gratefully acknowledge the financial support of the National Natural Science Foundation of China (22177032(J.L.)), National Key Research and Development Program of China (2023YFA0915402(J.L.)), and Natural Science Foundation in Hunan Province (2022RC3047(J.L.), 2021JJ10013(J.L.)) for financial support.

Author contributions

H.C., and J.L. conceived the experiments. H.C., J. L., and S.Z. performed the experiments and data analysis. H.C., and J.L. wrote the manuscript. All the authors including K.N., J.Z., X.H., J.H., K.W. and H.S. discussed the results and commented on the manuscript.

Competing interests

The authors declare no competing interests.

Additional information

Supplementary information The online version contains supplementary material available at https://doi.org/10.1038/s41467-024-53960-5.

Correspondence and requests for materials should be addressed to Jianbo Liu.

Peer review information *Nature Communications* thanks the anonymous reviewers for their contribution to the peer review of this work. A peer review file is available.